Design optimisation of braided composite beams for lightweight rail structures using machine learning methods

Anubhav Singh[a], Zewen Gu[b], Xiaonan Hou[b], Yiding Liu[a,*], Darren J. Hughes[a]

[a] WMG, University of Warwick, Coventry, CV4 7AL, UK

[b] Department of Engineering, Engineering Building, Lancaster University, Lancaster, LA1 4YW, UK

[*] Corresponding author. Email address: yiding.liu@warwick.ac.uk;

Abstract

Braided composites have seen substantial industrial uptake for structural applications in the past decade. The dependence of their properties on braid angle provides opportunities for lightweighting through structure-specific optimisation. This paper presents an integrated approach, combining finite element (FE) simulations and a genetic algorithm (GA) to optimise braided beam structures in the spaceframe chassis of a rail vehicle. The braid angle and number of layers for each beam were considered as design variables. A set of 200 combinations of these variables were identified using a sampling strategy for FE simulations. The results were utilised to develop a surrogate model using genetic programming (GP) to correlate the design variables with structural mass and FE-predicted chassis displacements under standard loads. The surrogate model was then used to optimise the design variables using GA to minimise mass without compromising mechanical performance. The optimised design rendered approximately 15.7% weight saving compared to benchmark design.

Keywords: Braided composites; Design optimisation; Genetic programming; Genetic algorithm; Lightweighting; Finite element analysis

1. Introduction

The last few decades have witnessed the transport industry coming under tremendous scrutiny owing to its contribution to carbon emissions, with some studies suggesting it is responsible for 24% of global CO_2 emissions [1]. Consequently, new legislations have been established, while existing ones have become more stringent. For instance, the UK government rescheduled its plan to ban the sale of internal combustion engine vehicles from 2030 to 2035 [2]. In order to comply with such legislative interventions, manufacturers across different industries (automotive, aerospace etc.) implemented technical innovations and/or upgraded their technological solutions. Principally, vehicle lightweighting is an obvious route towards reducing the carbon footprint over a product's lifetime. Moreover, the rapid uptake of powertrain electrification also requires the adoption of lighter vehicle bodies to accommodate the heavy battery modules and maximise the vehicle's range. In this regard, fibre reinforced composite materials are widely deployed in structural components as well as semi/non-structural components.

Owing to their superior mass-specific stiffness and strength, fibre reinforced polymer composites are used as substitutes for traditionally used steel and aluminium and continue to evolve with significant investments in industrial and academic research. An interesting composite manufacturing technology that has emerged is braiding. Inherently used for manufacturing hollow components, the braiding technology involves the interlacing of continuous fibres at an angle with respect to the local axis of the component. The angle at which the fibres are interlaced is termed as the braid angle. The automated nature of the process enables rapid manufacturing of near net-shape braided preforms that eliminate downstream trimming operations, thus minimising material wastage. Moreover, the interlaced network of reinforcement fibres provides superior resistance to damage propagation compared to planar laminated composites. Therefore, braided composites have been applied in a multitude of industries including aerospace, automotive and hydrogen storage.

Previous studies have demonstrated the use of controlled braid angle variation to achieve superior mechanical performance as well as lightweighting benefits [3–7]. This is a result of the significant dependence of mechanical (stiffness, strength, failure strain etc.) as well as physical properties (thickness, weight etc.) on braid angle [8–14]. These parameters combine to define the overall structural performance, therefore controlling the braid angle is an excellent avenue for tailoring braided composites without adding any cost or time to the braiding process.

In order to exploit the dependence of structural performance on manufacturing parameters, optimisation algorithms are often employed in the design of composite structures. Recently, evidence-based machine learning techniques have been used to replace the conventional numerical and experimental methods for investigating the single/mutual effects of the design variables and to arrive at the optimal design solution. A Genetic Algorithm (GA) is one of the promising machine learning techniques for aiding engineering research and applications [15–19]. Concurrently, the use of finite element (FE) simulations is becoming prominent in composite materials to reduce the reliance on costly non-standard experimental iterations. Therefore, several studies have employed an integrated approach combining optimisation algorithms with FE simulations. For instance, the optimisation of the stacking sequence for composite laminates with the objective of improving load-specific performance and/or minimising weight has been conducted using the abovementioned integrated approach [20–22]. A few studies have investigated optimisation of braided composite structures. Ghiasi et al. [23] used a local-global optimisation scheme in the design of a braided bicycle stem from a structural and manufacturing perspective. A structural simulation was used to model the mechanical behaviour of the stem under the part-specific load case, while a flow simulation was employed to visualise the resin flow during the moulding process. The results of the subsequent optimisation exercise produced multiple design variants that provided an informative insight into the compromise between three objectives, i.e., mechanical strength, weight and mould filling time. In a separate study, Eschler et al. [24] performed a multi-objective design optimisation for a braided automotive roof beam. The problem was defined using

four braiding parameters aimed at improving the local mechanical properties through the selective addition of axial tows. FE simulation results verified through limited experiments showed a 16% weight reduction while satisfying the required mechanical performance criteria. Whilst these studies demonstrated the effectiveness of multi-objective optimisation for braided composite structures, they did not consider braid angle as a parameter. Furthermore, the studies only considered the design of individual components without the context of the overall system. Therefore, the effects of the optimised design of the individual components on the overall structural performance could not be investigated, due to the lack of real boundary and loading conditions.

This paper presents a multi-objective optimisation exercise for improving the standard structural response of a recently developed light rail vehicle spaceframe chassis, as shown in Figure 1(a). The bottom chassis and side module beams are made of steel, and the upper chassis is composed of aluminium for weight reduction. In a recent research program entitled BRAINSTORM, the potential for substituting the beam components of the chassis with carbon fibre braided composites was investigated [25]. A modified chassis was designed with hollow beam structures to suit the inherent hollow tubular form of braided composites. While the results of the program from a manufacturing perspective were encouraging, aligned with the conventions of the composites industry, the project considered uniform braid angles of ±45°, i.e., a quasi-isotropic layup, for all the beams in the chassis. Thus, the resulting design was sub-optimal and did not exploit the potential offered by the correlation reported between properties and braid angle in previous studies [3-14]. As the structural performance is a combined outcome of material properties (dependent on braid angle) and geometry (dependent on braid angle and number of layers), this study investigates the potential of improving the structural efficiency, i.e., per unit weight mechanical performance, by considering different braid angles and number of layers in different beams across the structure. Figure 1(b) shows the modified chassis with beams considered in this study coloured green, while the geometric details of the beams are detailed in Figure 1(c). An integrated approach combining structural level FE simulations and Genetic Programming (GP) followed by a subsequent GA optimisation was used to find an optimal set of parameters that would result in minimum structural mass without compromising the required structural performance as defined by relevant vehicle standards. The results of the study demonstrate the potential benefits of optimising component-level design parameters while considering the performance of the overall structure as output. The study is also an attempt at structural level composite optimisation by exploiting the dependence of material properties on braid angle for braided composites.

2. Methodology

The conducted research is composed of three aspects: (*i*) analytical determination of composite properties, (*ii*) FE modelling of the structural response of the considered multi-material rail structure and (*iii*) GP and GA algorithms for correlating design and output variables as well as conducting an

iterative search of the most optimal solution to minimise structural mass under the structural performance boundaries defined by the standards. Figure 2 summarises the sequence of these work streams in the form of a flowchart. The green coloured highlighted beams shown in the spaceframe chassis were considered for substitution with braided composites. Roof cross-members and cant-rails were not selected for braided composite manufacture due to the resulting production difficulties. Therefore only five distinct side beams are required to be considered because of the symmetric geometry, as highlighted in Figure 2.

The design variables studied for the optimisation process in this paper included:

- the braid angles (θ_1, θ_2, θ_3, θ_4, θ_5) for the five beams and
- the number of layers (n_1, n_2, n_3, n_4, n_5) for the five beams,

resulting in a total of 10 design parameters. The static mechanical properties of the braided composite material required for the simulations were determined using an analytical algorithm. Similarly, the braid angle and number of layers were used to calculate the resulting beam thickness values for each category. Aligned with the conventional approach in composites industry, a design with an isotropic fibre angle profile, i.e., braid angle of 45°, and 5 braided layers in all the considered beams was selected as a benchmark. During the optimisation exercise, the discrete range of braid angle was selected from 30° to 60° with 5° interval, and the number of braided layers ranged from 3 to 9, selecting integral numbers only, as shown in Table 1. Therefore, the total number of possible combinations is 282,475,249 (7^{10}). The torsional and bending structural performance of the vehicle for a given design, i.e., a particular combination of the 10 parameters, was determined using FE simulations. Due to the significant computational cost and time, a sampling strategy based on Design of Experiments (DoE) was utilised to reduce the number of simulations to a total of 400 (200 each for torsional and bending loading design scenarios). The simulation results (maximum torsional and bending displacements of the vehicle, designated as u_{torsion} and u_{bending}) and the mass (mass of the considered beams, designated as M) pertaining to these 400 simulations were input into a GP algorithm with the respective design parameters. The GP algorithm produced a set of empirical relations correlating the design variables with the mechanical performance metrics and the structural mass of the considered braided composite beams. The relations were used as a surrogate of the FE model to generate the data required for the final GA-based optimisation algorithm, which resulted in a set of optimal design parameters. The results of the GA were also validated against the FE predicted values. The following section describes each step in further detail.

2.1 Analytical evaluation of mechanical properties of braided composites

Braided composites of comparable diameter as the beams being modelled in this work were manufactured and characterised by Cichoz et al. [26]. Based on the similarity in scale, braiding parameters and material properties reported in that study were selected to model the chassis beams. The composite was composed of Toho Tenax E HTS40 F13 12K carbon fibre tows in a Hexcel HexFlow

RTM6 epoxy resin. The material properties of the constituent fibre and matrix as well as the used braiding parameters are listed in Table 2. Here, E_{f1} and E_{f2} are the axial and transverse Young's modulus of the carbon fibre, G_{f12} is the shear modulus and ν_{f12} is the Poisson ratio. E_m and ν_m are the Young's modulus and Poisson ratio of the epoxy resin respectively. N is the total number of braiding carriers used, D is the braid outer diameter and Tex is the linear weight of the carbon fibre tows.

The analytical model proposed by Melenka et al. [27] was used to obtain the mechanical properties of the braided composites in this work. This was because the model results were reported to be in reasonable agreement with experimentally predicted material properties by Melenka et al. [27] for both diamond and regular braids for three different braid angles. Moreover, a higher prediction accuracy was reported for this model compared with equivalent models pertaining to the analytical determination of elastic constants for braided composite materials. The flowchart shown in Figure 3 summarises the algorithm behind the model. Firstly, the constituent properties listed in Table 2 were used to calculate the stiffness matrix of a tow using the rule of mixtures and Halpin-Tsai relations. Using the braiding parameters, the repetitive length of a tow in the braid was calculated. The tow stiffness matrix was transformed using a parametric formulation and integrated over the repetitive length to obtain the stiffness matrix in the tow coordinate system, which accounted for the undulation along the length of a braided tow. The undulation length was calculated as per Equation (1).

$$L = \frac{2\pi D}{N \sin\theta} \tag{1}$$

In this equation, L is the undulation length (mm), D is the braid outer diameter (mm), N is the number of braid carriers and θ is the braid angle (°). This was followed by a transformation to the global braid coordinate system, thus accounting for the inclination due to the braid angle. Finally, the rule of mixtures was employed to add the contributions of the two braided tows ($+\theta$ and $-\theta$) and the matrix that fills the inter-tow gaps. From the finally obtained stiffness matrix of the braid, the material properties were evaluated as per Equations (2)-(6).

$$\left[S_g\right]^{braid} = \left(\left[C_g\right]^{braid}\right)^{-1} \tag{2}$$

$$E_X = \frac{1}{S_g^{11}} \tag{3}$$

$$E_Y = \frac{1}{S_g^{22}} \tag{4}$$

$$G_{XY} = \frac{1}{S_g^{66}} \tag{5}$$

$$\nu_{XY} = \frac{-S_g^{12}}{S_g^{11}} \tag{6}$$

1   In these equations, $[C_g]^{braid}$ is the braid stiffness, matrix, $[S_g]^{braid}$ is the braid compliance matrix, E_X

2   is axial modulus, E_Y is transverse modulus, G_{XY} is shear modulus and v_{XY} is Poisson's ratio.

3   The thickness of the braided composites was predicted analytically. Assuming a 100% coverage, the

4   width of a braided tow is given as per Equation (7).

$$W = {2\pi D}/{N \cos \theta} \tag{7}$$

6   Using the Tex value corresponding to the fibre tow and its volume fraction in the braided tow, the

7   thickness was evaluated as per Equation (8). The thickness of the braided composite was obtained by

8   adding the individual tow thickness for every braided layer.

$$t = {0.004T}/{\pi \rho W V_t} \tag{8}$$

10   In these equations, W is the tow width (mm), t is the tow thickness (mm), T is the Tex of the carbon

11   fibre tows (g/km) and V_t is the fibre volume fraction within the tows. The consequently obtained

12   properties corresponding to different braid angles are shown in Figure 4. The axial modulus decreased

13   with increasing braid angle, while the transverse modulus showed the opposite trend. The shear modulus

14   was maximum for a braid angle of 45°. On the other hand, the thickness increased with braid angle,

15   which can be physically explained based on an increase in crimp at the fibre interlacement points as

16   well as a redistribution of the braided tows in the thickness direction because of tighter packing along

17   the circumference of the braided beam. All these observed trends were in agreement with previously

18   reported experimental data [9-11, 13,14].

19   **2.2 Finite element modelling of the rail structure**

20   The FE simulation model of the vehicle was created using Hypermesh code and the OptiStruct solver.

21   The vehicle model has been built from the three-dimensional (3D) geometry produced by a design

22   partner of the BRAINSTORM program [25]. A shell model was extracted by generating the mid-surface

23   from the 3D geometry to save computational cost/time. After conducting a mesh convergence study, an

24   element size of 10 mm was found appropriate. The entire steel bottom chassis was primarily joined by

25   welding, where RBAR elements were used in the model. The adhesive interfaces are bonded with the

26   adjacent components using tie constraints assuming a perfect bond with the surrounding materials. The

27   FE details of (a) beam connections with RBAR elements representative of welding, (b) multi-point

28   connections (MPC) in bogies mounts where boundaries were applied and (c) top chassis to roof panels

29   connections are illustrated in Figure 5.

30   The steel and aluminium substrates were modelled using isotropic material card (MAT1). The Young's

31   modulus and Poisson's ratio of steel and aluminium are 210 GPa/70 GPa and 0.3, respectively. The

32   braided composite material is modelled by orthotropic material card (MAT8), with the axial, transverse

33   and shear moduli and Poisson's ratio obtained from Figure 4 and explained in Section 2.1.

During the simultaneous optimization design of the braid angle and number of layers of the composite beams within the vehicle, two structural load scenarios were considered, i.e., torsional and bending loads, as shown in Figure 6. The loads are defined based on principles in GB-EN 12663-1 standard [28] for tramway vehicle category P-V. The torsional loading case was studied as it has been generally observed to result in the highest deformation in the vehicle body. The displacements and rotations were restricted at one end of the bogie mount connection point by rigid connections (RBE2 elements) to the surrounding nodes, with a total torsional load of 22,230 kN·mm applied to the other end. The torsional load was achieved by applying a positive and a negative load of a magnitude of 5.909 kN on the left and right side 11 nodes with a force arm of 342 mm. In that case, the vehicle is expected to exhibit a gradient deformation with the largest distortion at the nose-roof joint section. On the other hand, the bending rigidity was also simulated to test frame endurance at maximum payload from passenger and luggage of 56 kN weight to verify the robustness of the vehicle body. In the FE model, this was simulated by constraining the four wheels, i.e., bogie mounts as fully fixed supports, while a uniform downward load of 56 kN was applied on the Centre of Gravity (CoG) of the entire vehicle (1.298 m above the bottom surface of the vehicle), distributed evenly on the lower chassis with RBE3 connections. To match the realistic vehicle structural mass, non-structural masses distributed within the relevant location are added to the vehicle structure using RBE3 elements to link the mass with the surrounding elements, e.g., battery box, mid compartment and HVAC, etc. Based on preliminary trials, both analyses were expected to work within elastic conditions for the two considered load states. Therefore, a linear elastic solver was assumed to be appropriate for the simulations.

The maximum displacements obtained from the simulations pertaining to the two structural cases, defined as $u_{torsion}$ and $u_{bending}$, were used as performance metrics and output variables. The maximum displacements were observed at the nose-roof joint section and the centre of the lower chassis for the two loading cases respectively. These maximum displacements are the key targets to be compared with the benchmark design, as described in the Section 2 and would be used eventually to calculate the torsional and bending stiffnesses of the vehicle. Torsional stiffness is the characteristic property of a structure which signifies how rigid and how much resistance the structure offers per degree change in its angle when twisted, as shown in Equation (9). Bending stiffness is the ratio of bending moment to rotation or moment required to cause unit rotation, as defined in Equation (10). The combined mass (m) of all the designed beams, which is the optimisation objective compared to the benchmark design (with a mass of 61.71 kg), was also measured from the FE simulations. It can be seen that even though the structural components are the same in different loading cases, their positions are changed which results in differences in the vehicle performance. Thus, multiple FE models need to be established for all loading cases.

For calculating torsional stiffness:

1. $$K_{torsion} = {}^{T}\!/\!{}_{tan^{-1}(2u_{torsion}/W)} \tag{9}$$

2. In the equation, T is the torsional load in N, and $u_{torsion}$ is the deflection under torsional load in mm, W

3. is the distance between the centre of the two bogies, which is 7600 mm.

4. For calculating bending stiffness:

5. $$K_{bending} = {}^{F}\!/\!{}_{u_{bending}} \tag{10}$$

6. In this equation, F is the total force applied at CoG (56 kN), and $u_{bending}$ is the deflection under bending

7. load in mm.

8. This vehicle design work is part of the Coventry Lightweight Rail (CVLR) project, where the FE model

9. of the detailed carbody has been peer-reviewed and the vehicle's prototype demonstrator was

10. manufactured successfully. Therefore, the validability of the numerical simulation can be trusted. The

11. modelling work was carried out using a 64-bit operating processor workstation, the running time for

12. each model is approximately180 s for the static analysis.

13. **2.3 Machine learning models**

14. *2.3.1 Sampling strategy*

15. Data-based approaches require an appropriate data set from a specific problem domain for the purpose

16. of accurate training and testing. It is expected that the selected dataset is a representative of the

17. properties of the entire problem domain. Similarly, in this study, the surrogate developed using the GP

18. algorithm is expected to capture the resulting performance metrics from all the possible combinations

19. of design parameters. Therefore, it is crucial to generate a near-random and appropriately spread set of

20. data points from a multidimensional distribution. In this study, the standard Latin Hypercube Sampling

21. (LHS) DoE technique, which is a stratified sampling method and considered superior over the

22. traditional random sampling method, was adopted. The algorithm of LHS was coded in the commercial

23. software MATLAB, and the primary principles of the standard LHS can be considered as follows [18]:

24.   a. The set of the d input dimension $x = (x_1, x_2 ,…, x_d)_T$ is divided into N equal intervals, and only

25.   one experiment is allowed in each interval.

26.   b. When providing a dimension, k, only one sample exists in each interval and thus N scalar

27.   samples are generated.

28.   c. By randomly matching these scalar samples in the ith dimension k_i, a N dimensional tuple $X_1, …,$

29. X_N can be obtained.

30.   d. Calculate the probability of the LHS using the same method as the Monte Carlo.

31. The detailed working principles of LHS and its benefits in selecting numerical samples can also be

32. found in previous studies [18].

In this study, a total of ten discrete design variables including the braid angle (θ_i) and the number of braided layer (n_i) of five designated side beams are defined (see Fig. 2). Based on the definitions of these variables, LHS was implemented to generate samples with different combinations of the variables.

In total, a database of 200 sets of sample points was generated in the constrained domain for the torsional and bending cases respectively. The total computation efforts for the FE work were 10 hours. Based on the FE modelling described in Section 2.2, a group of output variables ($u_{torsion}$ and $u_{bending}$) can be achieved for further learning and optimisation work, as shown in Figure 7. It can be seen that $u_{torsion}$ ranges widely from 60 mm to 90 mm and $u_{bending}$ has a relatively small range from 20 mm to 23 mm, which means the vehicle's torsional performance is more sensitive to the designed parameters of the side beams compared to the bending performance. However, both output variables have reasonably random distributions. It should be noted that the structural mass (M) for each design variables measured from FE modelling were also learnt and produced for optimisation work.

2.3.2 GP

GP is a subarea of evolutionary algorithms, which is inspired by Darwin's theory of evolution. It can be used to find the relationship among variables in the data sets. Unlike building empirical models, which is usually problematic in selecting the structure of the approximation function, the GP technique is a systematic and efficient way of searching for high-quality global approximations. Generally, GP is a tree-structure based algorithm to exploit desired solutions from all the satisfied expressions, of which a process flowchart is displayed in Figure 8. Koza [29] identified five preliminary steps to solve a problem using GP, including choosing the terminals, the functions, the fitness function, the control parameters and the termination criterion. First, the structure of programs is initialized to allow the insertion of the parameters, which will later form the first parents population. Then, the evaluation of the fitness is conducted, which determines the quality of the approximations of the current generation. For the next step, the individuals of the parents generation will evolve by employing tuning algorithms. The commonly used tuning algorithms in GP are mutation and crossover, which perform on the connections between mathematical operators and the terminal nodes. At the end, the evolved individuals from the child generation become the next parent generation after evaluating the fitness. The whole process terminates only when the value of fitness reaches an acceptable level. The final mathematical expressions determined by the tree structure program can be one of the approximation functions that is searched for.

The GP model is implemented by using the Python package 'GPlearn'. The parameters of the GP model used for regressing the current function are listed in Table 3. As shown in the table, five operators are used in the function set. A group of 150 randomly selected samples from the 200 sets of FE results for each loading scenarios are used for training the GP model. The remaining 50 sets of the FE results are

1 used as the independent test sets to demonstrate the validity and accuracy of the trained GP model. The

2 equations of the GP model are shown in the appendix.

3 *2.3.3 GA optimisation scheme*

4 Genetic algorithm (GA) is a prospective machine learning technique for aiding engineering

5 optimisation. It is a non-deterministic stochastic search method that utilises the theories of evolution

6 and natural selection to solve a problem within complex solution spaces [30,31]. The spread of GA has

7 demonstrated its benefits in solving complicated composite design optimisation during the past few

8 years. The objective of the design optimisation in this study was to find a combination of the design

9 parameters, i.e., braid angles and number of layers for each beam resulting in minimum structural mass.

10 Traditionally, the composites industry prefers a quasi-isotropic layup, i.e., layup with equivalent

11 properties along the two planar directions. This simplifies structural modelling and also avoids

12 unwanted coupling in the structure. However, the resulting composite would be overdesigned and hence

13 carries undesired weight. Therefore, in the current optimisation study, a configuration with 5 layers of

14 quasi-isotropic 45º braid angle in every beam was considered as the benchmark against which the

15 optimisation constraints were defined. The optimisation study could be summarised using the equations

16 below, with Equation (11) defining the target, while Equations (12) and (13) define the constraints.

17 Here, M represents the structural mass of the braided vertical beams, $u_{\text{torsion}}^{\text{BM}}$ and $u_{\text{bending}}^{\text{BM}}$ represent

18 the torsional and bending displacements corresponding to the benchmark design, while u_{torsion} and u_{bending}

19 are the displacements corresponding to any design with a particular combination of design parameters.

20 $\text{minimise}(M)$ (11)

21 *Subject to:*

22 $u_{torsion} \leq u_{torsion}^{BM}$ (12)

23 $u_{\text{bending}} \leq u_{bending}^{BM}$ (13)

24 Figure 9 shows the working of the GA during the optimisation exercise based on the abovementioned

25 problem. The GA algorithm is achieved by employing the Python package 'Geatpy'. To initiate the GA,

26 a random population with 1500 candidate solutions, i.e., combinations of the 10 design parameters was

27 generated. Corresponding to each candidate, the three output variables, i.e., mass and the two chassis

28 displacements were evaluated using the surrogate model. Based on these calculated values, the

29 algorithm estimates the objective function value for each candidate solution, i.e., the mass. However,

30 to honour the two constraints pertaining to the displacements, the objective function value is penalised

31 for a candidate solution if the constraints are violated. Following the objective function determination,

32 two selection strategies, namely elitism and tournament selection were employed to select parents from

33 the initial population. Genetic operators of crossover and mutation were applied to create the next

34 generation from the parents, for which the masses were calculated and the whole process is repeated.

1   Thus for every subsequent generation, the mass was reduced while respecting the two constraints. Table

2   4 summarises the settings used in the GA optimisation.

3   **3. Results and discussion**

4   **3.1 Results of surrogate model**

5   The cross plotting of the mass, u_{torsion} and u_{bending} obtained from the GP estimated training results and

6   the predicted testing results from FE modelling are presented in Figure 10. The validation line is defined

7   where the values predicted by the surrogate match those from the FE simulations. In the training phase,

8   the GP model could learn from the data samples efficiently with higher correlation as almost 95% of

9   the data falls close to the validation line. For the testing phase, the corresponding R^2 values for mass,

10   u_{torsion} and u_{bending} are 0.90, 0.90, 0.94 respectively, which suggests reasonable agreement between the

11   surrogate model and the FE simulations. It can be seen that a few data points are distant from the

12   validation, which represents relatively poor correlations. These values could be further improved if the

13   complexity of the function set in the GPlearn is improved, which will however significantly increase

14   the computing time and lift the difficulties of converging of the GP model.

15

16   **3.2 Optimal solution from GA**

17   Figure 11 shows the evolution of the objective function, i.e., total structural mass of the braided beams

18   for every generation. The mass showed a significant drop up to the 150th generation, beyond which the

19   change was relatively negligible. Moreover, the difference between the average and best objective

20   function, i.e., mass was negligible beyond approximately the 200th generation, which indicates that the

21   algorithm converged to the target solution.

22

23   The design parameters corresponding to the best candidate solution at the termination point, the 500th

24   generation, are shown in Table 5.

25

26   Compared to the benchmark quasi-isotropic composite layup (θ of 45º and n of 5), the obtained

27   optimised solution showed a mass reduction of approximately 15.7% based on the analytical relations,

28   from 61.71 kg of benchmark design to 52.03 kg, as shown in Table 6. The displacements u_{torsion} and

29   u_{bending} decreased by 6.3% and 0.8%, respectively which resulted in a 6.7% increase of torsional stiffness

30   from 5136.99 N/deg to 5482.53 N/deg and a 0.8% increase of bending stiffness from 2554.74 N/mm to

31   2575.90 N/mm. In order to verify the findings based on the GP's analytical relations and the subsequent

32   GA based optimisation, the results were verified against FE simulations. The results of the FE validation

33   exercise comparing the GA optimised design and benchmark design are shown in Figure 12. The stress

34   contours of the GA optimised design are shown in Figrue 13 for examining the vehicle's performance.

35   The corresponding errors in the prediction of the three metrics for both the designs are listed in Table

36   6. It can be seen that the GP predicted mass has a slightly larger difference of 2.85% compared to the

FE validation, this could be due to the error from the surrogate model which is responsible to the deviation obtained in the GA optimisation route. However, based on the minimal error (less than 3%) in the predicted results, the results indicate a successful optimisation study via the proposed machine learning approach.

4. Conclusions

In this paper, the beam structures in the spaceframe chassis of a light rail public transport vehicle were considered for a material substitution with braided composites and an optimisation study was presented to minimise their structural mass. A combination of structural FE simulations and GA based algorithms was utilised. A conventional design with a homogenous quasi-isotropic fibre layup in each beam was selected as the benchmark. The design parameters consisted of braid angle and number of layers for five designated beams, while the maximum chassis displacements under torsional and bending loads corresponding to the benchmark design served as constraints. In order to minimise computation time, a GP algorithm was used to develop a surrogate model relating the design parameters with weight (objective function) and the two chassis displacements (constraints). The surrogate model was then used in a GA-based optimisation algorithm to evaluate the weight and chassis displacements corresponding to each design. The GA algorithm terminated after 500 generations of 1500 possible designs. A weight saving of 15.7% with respect to the benchmark design was achieved in the optimised design, from 61.71 kg to 52.03 kg. This also resulted in a 6.7% increase of torsional stiffness from 5136.99 N/deg to 5482.53 N/deg and a 0.8% increase of bending stiffness from 2554.74 N/mm to 2575.90 N/mm. The GP predicted results corresponding to the optimal design were revalidated using the FE model and an error of less than 3% was found.

The performed study shows the effectiveness of machine learning algorithms in optimising the design of individual composite components while considering the performance of the entire structure. Moreover, the study also highlights the potential to exploit the dependence of properties on braid angle, thus strengthening the case for the application of braided composites for beam structures. The authors believe that future work considering triaxial braids as well as other multi-material structures in domains of aerospace, automotive etc, would expand the potential design improvements presented in this study and improve the uptake of braided composites as well as the use of combined simulation and machine learning approaches in the industry.

Appendix

The equations for the mass (M), $u_{torsion}$ and $u_{bending}$ obtained from the GP prediction are listed here.

M = mul(mul(n_2, sqrt(mul(n_4, -0.014))), mul(0.030, add(n_3, div(mul(θ_2, sqrt(mul(n_5, mul(sqrt(mul(n_1, mul(div(mul(n_5, mul(sqrt(n_3), mul(mul(n_2, sqrt(mul(sqrt(mul(sub(θ_3, mul(mul(n_2, mul(mul(θ_4, div(mul(n_5, mul(mul(n_2, sqrt(mul(n_4, -0.014))), mul(mul(n_2, sqrt(n_4)), mul(mul(mul(θ_4, div(mul(θ_4, div(θ_3, n_2)), n_2)), sqrt(mul(n_4, -0.014))), mul(0.030, add(mul(n_2, sqrt(sqrt(θ_3))), n_1)))))))), n_2)), sub(θ_3, sqrt(mul(θ_4, sub(θ_3, mul(mul(n_2, sqrt(div(n_5, n_3))), sqrt(mul(sqrt(add(θ_3, mul(θ_2, sub(θ_3, n_2)))), div(θ_3,

12

1 n_3)))))))))), mul(0.030, add(n_3, div(mul(mul(mul(sqrt(mul(div(n_5, 0.763), sub(n_2, θ_1))),

2 mul(sqrt(sqrt(mul(-0.952, add(add(mul(n_2, mul(div(sqrt(n_4), n_2)), mul(mul(sqrt(add(θ_3, n_3)),

3 mul(sqrt(sqrt(mul(sub(n_2, n_1), sub(n_2, θ_1)))), div(θ_5, n_5))), mul(sqrt(sqrt(n_3)), mul(mul(sqrt(sub(n_2, θ_1)),

4 div(θ_5, n_5)), sqrt(div(n_5, n_3)))))))), n_4), n_1)))), div(θ_5, n_5))), mul(sqrt(sqrt(div(n_5, n_3))), div(θ_5, n_5))), -

5 0.014), n_2)))))), sub(θ_3, sqrt(mul(θ_4, div(θ_2, n_2))))))), -0.014))), mul(0.030, add(n_3,

6 add(sqrt(mul(sqrt(sub(θ_3, θ_4)), mul(add(add(mul(n_2, mul(θ_1, mul(mul(mul(n_2, sqrt(mul(n_4, -0.014))),

7 mul(sqrt(sqrt(mul(sub(n_2, n_1), sqrt(div(θ_5, n_5))))), div(θ_5, n_5))), mul(sqrt(mul(sqrt(n_5), sub(n_2, θ_1))),

8 div(θ_5, n_5))))), n_4), n_1), θ_2))), n_2)))))), n_2), mul(mul(mul(θ_4, div(mul(θ_4, sqrt(mul(mul(θ_1, mul(sqrt(n_5),

9 mul(sqrt(sqrt(mul(n_4, -0.014))), div(θ_5, n_5)))), sub(θ_3, sqrt(add(θ_3, n_3)))))), n_2)),

10 sqrt(mul(sqrt(mul(sub(θ_3, mul(mul(div(n_5, θ_2), mul(mul(θ_4, div(mul(n_5, mul(mul(n_2, sqrt(sqrt(mul(n_4,

11 -0.014)))), sqrt(θ_3)), n_2)), sub(θ_3, mul(0.030, add(n_3, add(sub(θ_3, mul(div(θ_5, n_5)), mul(mul(-0.952, n_1),

12 mul(n_5, θ_5)))), add(n_3, sqrt(mul(n_5, θ_5)))))))))), mul(0.030, add(n_3, div(θ_2, add(θ_3, mul(sub(n_2, n_1),

13 sub(n_2, θ_1)))))))), sub(θ_3, sqrt(mul(θ_4, sub(θ_3, mul(mul(n_2, sqrt(sqrt(div(n_5, n_3)))), sqrt(mul(sqrt(add(θ_3,

14 mul(θ_2, sub(θ_3, sqrt(add(add(θ_3, sqrt(sqrt(div(n_4, θ_2)))), n_3)))))), div(θ_3, n_3))))))))))), -0.014))),

15 mul(0.030, add(n_2, sqrt(sqrt(θ_2))))))))), div(θ_3, n_3))))), n_2))))

16 $\boldsymbol{u_{torsion}}$ = div(sqrt(sqrt(div(div(add(div(sub(add(θ_3, θ_1), add(n_4, θ_1)), add(sqrt(n_2), div(n_2, n_5))), θ_4),

17 div(n_4, θ_5)), sqrt(div(-0.988, n_2)))))), sqrt(div(add(n_4, n_3), sqrt(mul(div(θ_2, n_5),

18 sqrt(div(mul(add(mul(div(θ_2, n_5), sqrt(div(mul(add(n_2, sqrt(n_5)), div(add(add(n_4, n_3), div(n_4, n_5)),

19 sqrt(div(mul(sqrt(mul(θ_5, θ_2)), sqrt(add(n_4, θ_1))), sqrt(sqrt(n_4)))))), div(add(div(div(sqrt(mul(θ_5,

20 add(sqrt(θ_4), θ_3))), sqrt(mul(mul(n_4, n_5), sub(θ_2, n_5)))), div(-0.988, n_2)), θ_4), div(n_3, θ_5))))), add(θ_1,

21 add(div(add(div(θ_1, n_3), θ_4), div(n_2, θ_2)))), sqrt(mul(sqrt(θ_3), div(add(div(sqrt(sqrt(sqrt(-0.580))),

22 sqrt(div(add(n_4, n_3), sqrt(n_2)))), mul(div(add(div(n_2, θ_2), add(div(add(θ_1, n_3), θ_4), div(n_2, θ_2))), n_5),

23 sqrt(div(mul(add(θ_3, sqrt(n_4)), div(add(sqrt(n_2), add(div(n_2, n_5), θ_4), div(n_2, θ_2))),

24 sqrt(div(mul(div(sub(add(θ_3, θ_1), div(add(sqrt(add(-0.412, div(n_4, θ_5))), div(n_2, n_5)), sqrt(div(0.191,

25 n_3)))), sqrt(div(mul(add(sqrt(θ_3), sqrt(n_4)), div(add(sqrt(n_2), add(div(add(sqrt(mul(-0.901, θ_2)), div(n_2,

26 θ_2)), θ_4), div(n_2, θ_2))), sqrt(div(mul(div(sub(add(θ_3, θ_1), div(add(sqrt(add(-0.412, div(θ_2, n_5))), div(n_2,

27 n_5)), sqrt(div(0.191, n_3)))), add(sqrt(mul(-0.901, θ_2)), div(n_2, θ_2))), add(sub(θ_2, 0.623), add(n_2, n_3))),

28 add(n_4, θ_1))))), add(div(sub(add(θ_3, θ_1), sub(mul(n_4, n_3), add(n_1, sub(add(θ_2, 0.836), add(θ_4,

29 add(sqrt(θ_4), θ_3)))))), add(sqrt(mul(-0.901, θ_2)), div(n_2, θ_2))), θ_4)))), add(sub(θ_2, 0.623), add(n_2, n_3))),

30 add(add(n_4, θ_1), div(n_2, θ_2)))))), add(div(sub(add(θ_3, θ_1), sub(mul(n_4, n_3), add(n_1, sub(add(θ_2, 0.836),

31 add(θ_4, add(θ_3, θ_1)))))), add(sqrt(mul(-0.901, θ_2)), div(n_2, θ_2))), θ_4)))),

32 sqrt(div(div(add(div(mul(mul(n_4, n_5), sub(θ_2, n_5)), n_5), θ_4), div(n_4, θ_5)), sqrt(div(-0.988, n_2)))))))))), add(-

33 0.412, n_4))))))))

34 $\boldsymbol{u_{bending}}$ = sqrt(div(sqrt(div(add(mul(div(sub(n_4, div(θ_1, θ_3)), θ_4), -0.019), add(mul(div(n_4, div(θ_4,

35 sqrt(sqrt(sub(n_4, sqrt(div(sqrt(div(sqrt(θ_4), div(n_2, n_4))), sqrt(div(sqrt(div(sqrt(div(div(sqrt(sub(n_3,

36 add(div(sub(n_3, add(sqrt(div(n_2, n_4)), div(θ_3, θ_5))), div(div(θ_3, n_4), θ_4)), div(sqrt(sqrt(sqrt(add(n_4, n_5)))),

37 sqrt(sub(n_3, div(θ_2, θ_2)))))))), div(n_4, θ_4)), div(n_2, n_4))), sub(n_4, sqrt(div(sqrt(div(div(sqrt(sub(n_4,

38 sqrt(sub(sqrt(div(sub(n_3, div(sqrt(div(add(n_1, θ_2), div(n_4, θ_4))), sqrt(sqrt(n_4)))), mul(n_5, -0.019))),

39 add(mul(-0.765, sqrt(sub(n_3, add(sqrt(θ_4), sub(n_3, add(div(sub(n_3, add(div(n_2, n_4), div(θ_3, θ_5))),

40 div(div(θ_3, n_4), θ_4)), sqrt(n_4))))))), div(θ_3, θ_5))))), div(n_4, θ_4)), div(n_2, n_4)))), sqrt(div(n_2,

41 n_4)))))))))), -0.019), div(θ_3, n_4))), div(n_4, θ_4))), sqrt(sub(n_3, sqrt(sub(sqrt(div(sub(n_3,

42 div(sqrt(div(add(n_1, θ_2), div(n_4, θ_4))), sqrt(sqrt(n_4)))), mul(n_5, -0.019))), add(mul(-0.765, sqrt(sub(n_3,

43 add(sqrt(θ_4), sub(n_3, add(div(sub(n_3, add(sqrt(div(n_2, n_4)), div(θ_3, θ_5))), div(div($\theta_3\theta_3$, n_4), θ_4)),

44 sqrt(div(sub(sqrt(sub(θ_4, sqrt(n_4))), div(n_4, θ_4)), div(n_2, n_4)))))))))), div(θ_3, θ_5)))))))

45 where θ_1, θ_2, θ_3, θ_4, θ_5 are the braid angles for five beams and n_1, n_2, n_3, n_4, n_5 are the number of layers

46 for five beams.

1 Acknowledgements

2 The authors are thankful to the technical staff at WMG and Lancaster University for their time and

3 support in this work. The authors are grateful to Dr Craig Carnegie for his time with the preparation of

4 the manuscript. The vehicle structure was designed in collaboration with WMG by TDI Ltd, UK.

5 References

6 [1] International Energy Agency (IEA). Tracking Transport 2020. 2020. Available from:
7   https://www.iea.org/reports/tracking-transport-2020. Date accessed: 5th May, 2021.
8 [2] UK Goverment. Government takes historic step towards net zero with end of sale of new
9   petrol and diesel cars by 2030. 2020.
10   Available from: https://www.gov.uk/government/news/government-takes-historic-step-
11   towards-net-zero-with-end-of-sale-of-new-petrol-and-diesel-cars-by-2030. Date accessed: 5th
12   May, 2021.
13 [3] Ganesh VK, Choo TS. Modulus graded composite adherends for single-lap bonded joints. J
14   Compos Mater 2002;36:1757–67.
15 [4] Boss JN, Ganesh VK. Fabrication and properties of graded composite rods for biomedical
16   applications. Compos Struct 2006;74:289–93.
17 [5] Huang Z-M, Wang Q, Ramakrishna S. Tensile behaviour of functionally graded braided
18   carbon fibre/epoxy composite material. Polym Polym Compos 2002;10:307–14.
19 [6] Stanier D, Radhakrishnan A, Gent I, Roy SS, Hamerton I, Potluri P, et al. Matrix-graded and
20   fibre-steered composites to tackle stress concentrations. Compos Struct 2019;207:72–80.
21 [7] Singh A, Reynolds N, Keating EM, Barnett AE, Barbour SK, Hughes DJ. Three-point flexural
22   performance of tailor-braided thermoplastic composite beam structures. Compos Struct
23   2021;260:113521.
24 [8] Wehrkamp-Richter T, Hinterhölzl R, Pinho ST. Damage and failure of triaxial braided
25   composites under multi-axial stress states. Compos Sci Technol 2017;150:32–44.
26 [9] Harte AM, Fleck NA. On the mechanics of braided composites in tension. Eur J Mech
27   A/Solids 2000;19:259–75.
28 [10] Laberge-Lebel L, Van Hoa S. Manufacturing of braided thermoplastic composites with
29   carbon/nylon commingled fibers. J Compos Mater 2007;41:1101–21.
30 [11] Potluri P, Manan A, Francke M, Day RJ. Flexural and torsional behaviour of biaxial and
31   triaxial braided composite structures. Compos Struct 2006;75:377–86.
32 [12] Singh A, Reynolds N, Keating EM, Barnett AE, Barbour SK, Hughes DJ. The effect of braid
33   angle on the flexural performance of structural braided thermoplastic composite beams.
34   Compos Struct 2020:113314.
35 [13] Kohlman LW, Bail JL, Roberts GD, Salem JA, Martin RE, Binienda WK. A notched coupon
36   approach for tensile testing of braided composites. Compos Part A Appl Sci Manuf
37   2012;43:1680–8.
38 [14] Gautam M, Potluri P, Ogin S, Jain P. Necking behaviour of flattened tubular braided
39   composites. In: ICCM 2015: Proceedings of the 20th International Conference on Composite
40   Materials, Copenhagen, July 2015.
41 [15] An H, Chen S, Huang H. Optimal design of composite sandwich structures by considering
42   multiple structure cases. Compos Struct 2016;152:676–86.
43 [16] An H, Chen S, Huang H. Simultaneous optimization of stacking sequences and sizing with
44   two-level approximations and a genetic algorithm. Compos Struct 2015;123:180–9.
45 [17] Pelletier JL, Vel SS. Multi-objective optimization of fiber reinforced composite laminates for
46   strength, stiffness and minimal mass. Comput Struct 2006;84:2065–80..
47 [18] Liu Y, Gu Z, Hughes DJ, Ye J, Hou X. Understanding mixed mode ratio of adhesively bonded
48   joints using genetic programming (GP). Compos Struct 2021;258:113389.
49 [19] Gu Z, Liu Y, Hughes D, Ye J, Hou X. A parametric study of adhesive bonded joints with
50   composite material using black-box and grey-box machine learning methods: Deep neuron
51   networks and genetic programming. Compos Part BEngineering 2021;108894.

14

[20]   Schatz ME, Hermanutz A, Baier HJ. Multi-criteria optimization of an aircraft propeller considering manufacturing. Struct Multidiscip Optim 2017;55:899–911.

[21]   Airoldi A, Bertoli S, Lanzi L, Sirna M, Sala G. Design of a motorcycle composite swing-arm by means of multi-objective optimisation. Appl Compos Mater 2012;19:599–618.

[22]   Farzan Nasab F, Geijselaers HJM, Baran I, Akkerman R, de Boer A. Optimization of the Interacting Stiffened Skins and Ribs Made of Composite Materials. AIAA J 2020;58:1836–50.

[23]   Ghiasi H, Lessard L, Pasini D, Thouin M. Optimum structural and manufacturing design of a braided hollow composite part. Appl Compos Mater 2010;17:159–73.

[24]   Eschler E, Miadowitz T, Zaremba S, Drechsler K. Design optimization of a braided roof frame reinforcement by process-integrated local customization of component properties. Appl Compos Mater 2020:1–17.

[25]   Warwick University News. Minister shown how WMG literally weaved design of Very Light Rail – Braided structure is super lightweight. 2019. Available from: https://warwick.ac.uk/newsandevents/pressreleases/minister_shown_how/. Date accessed: 5th May, 2021.

[26]   Cichosz J, Wehrkamp-Richter T, Koerber H, Hinterhölzl R, Camanho PP. Failure and damage characterization of (±30°) biaxial braided composites under multiaxial stress states. Compos Part A Appl Sci Manuf 2016;90:748–59.

[27]   Melenka GW, Carey JP. Development of a generalized analytical model for tubular braided-architecture composites. J Compos Mater 2017;51:3861–75.

[28]   European Committee for Standardization. EN 12663-1:2010+A1:2014 Railway applications - Structural requirements of railway vehicle bodies - Part 1: Locomotives and passenger rolling stock (and alternative method for freight wagons). 2010.

[29]   Koza JR. Genetic programming as a means for programming computers by natural selection. Stat Comput 1994;4:87–112.

[30]   Bhoskar T, Kulkarni OK, Kulkarni NK, Patekar SL, Kakandikar GM, Nandedkar VM. Genetic Algorithm and its Applications to Mechanical Engineering: A Review. Mater Today Proc 2015;2:2624–30.

[31]   Pisinger D, Ropke S. A general heuristic for vehicle routing problems. Comput Oper Res 2007;34:2403–35.

(a) Main components in the vehicle   (b) Simplified spaceframe chassis studied in this paper

(c) Geometric dimensions of the selected beams in detail (unit in m)
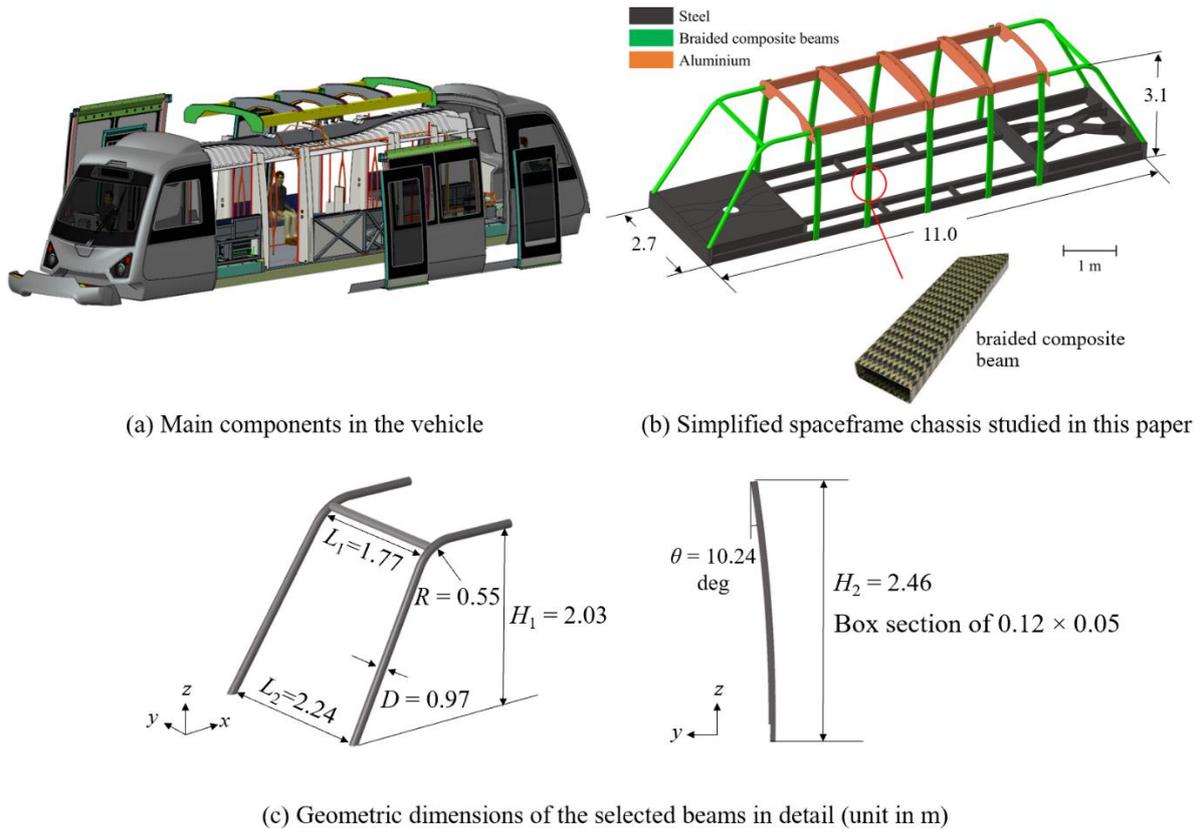
Figure 1 (a) Exploded view of the main components in the rail vehicle; (b) simplified spaceframe chassis composed of tubular beams studied in this paper; (c) geometric parameters of the selected beams shown in detail. All units are in m.

Braid angle					Number of layers				
θ_1	θ_2	θ_3	θ_4	θ_5	n_1	n_2	n_3	n_4	n_5
55	35	30	35	35	6	9	8	4	6
35	35	55	50	45	4	3	4	8	6
55	55	35	35	45	8	8	5	7	8
45	50	45	30	45	9	5	9	8	5
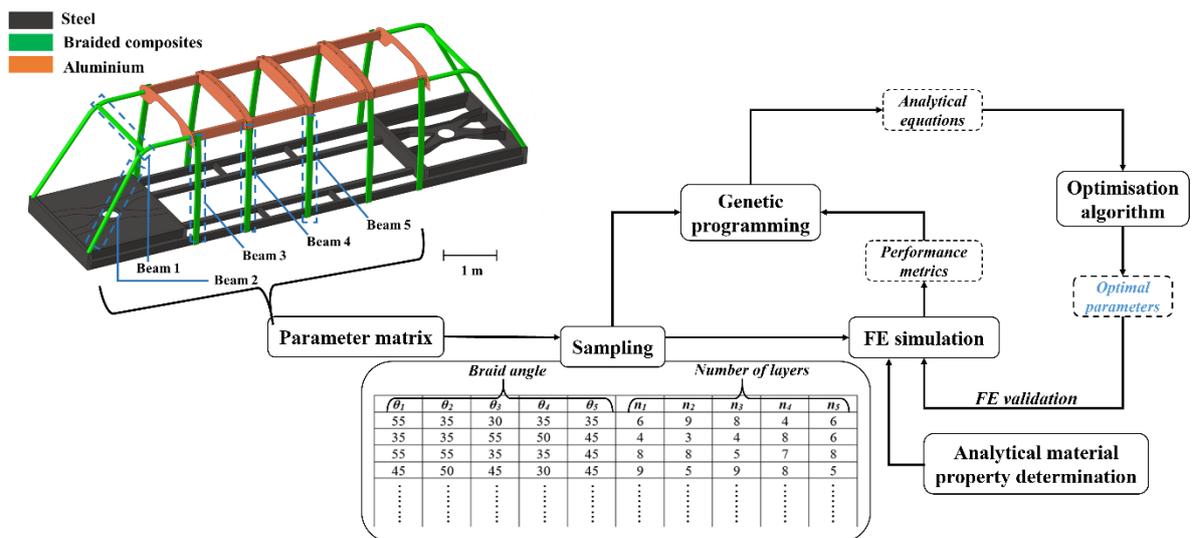
Figure 2 Flowchart of overall approach with different components.

The following boxes and equations appear within the figure:

Tow mechanical properties: Rule of mixtures and Halpin-Tsai relations

Stiffness matrix *[C]*

Constituent properties: Fibre and matrix

Transformation of tow stiffness matrix to local tow coordinate system

Integration along repetitive undulation length

$$[C_t] = \frac{1}{L}\int_0^L [T_c]^{-1}[C][R][T_c]'R^{-1}dx$$

Transformation of integrated tow stiffness matrix to global braid coordinate system

$$[C_g] = [T_g]^{-1}[C_t][R][T_g]'R^{-1}$$

Addition of tow and matrix properties to obtain braided composite stiffness matrix

$$[C_g]^{braid} = V_m[C]^m + V_f^{+\theta}[C_g]_{+\theta}^{tow} + V_f^{-\theta}[C_g]_{-\theta}^{tow}$$

Glossary:

$[C_t]$: Tow stiffness matrix in tow coordinate system

$[C_g]$: Tow stiffness matrix in global braid coordinate system

$V_f^{+\theta}$: Volume fraction of tow aligned along $+\theta$

V_m: Volume fraction of resin (matrix) present between tows

$[C]^m$: Stiffness matrix of resin

$[C_g]^{braid}$: Overall stiffness matrix of braid

Figure 3 Analytical algorithm for determination of braided composite material properties. Adapted from [27].
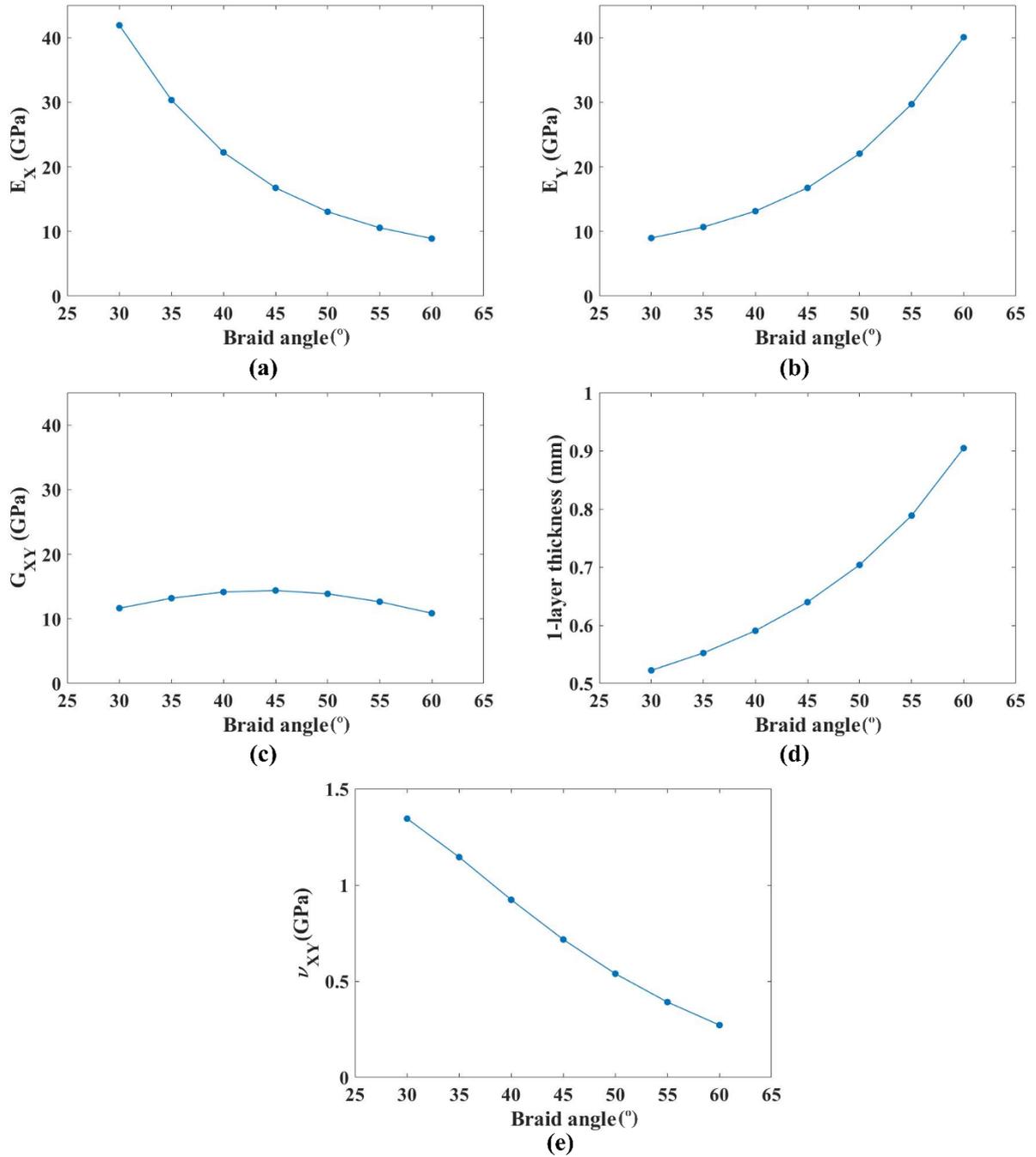
Figure 4 Analytically obtained (a) axial modulus, (b) transverse modulus, (c) shear modulus, (d) single layer thickness and (e) Poisson's ratio corresponding to different braid angles.
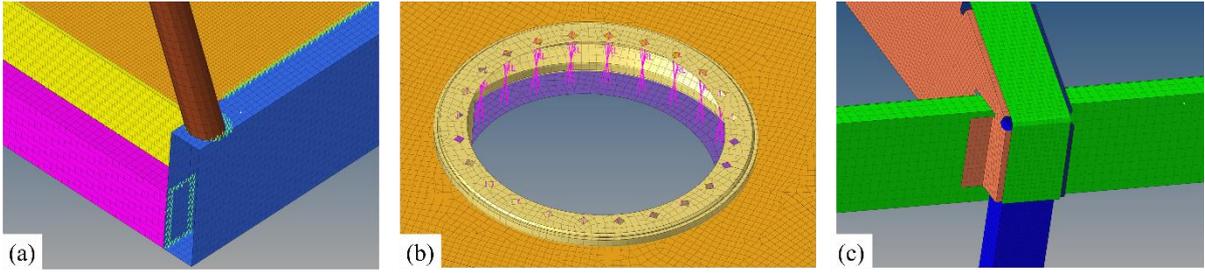
Figure 5 FE details of (a) beam connections with RBAR elements representative of welding, (b) multi-point connections (MPC) in bogies mounts where boundaries were applied, (c) top chassis to roof panels connections.

(a) Torsional Rigidity

(b) Bending Rigidity
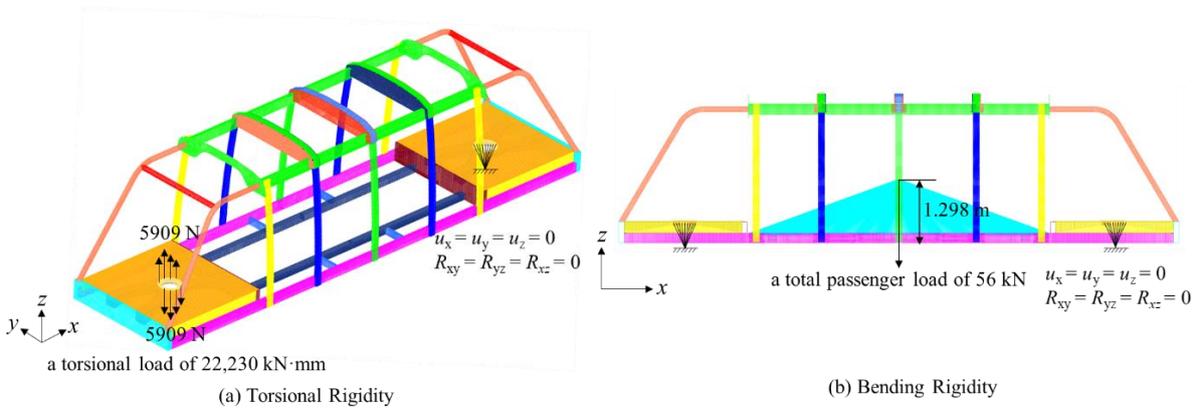
Figure 6 FE modelling of the vehicle under (a) torsional and (b) bending load scenario, the structural cases are designed according to the EN 12663 standard.

(a) $u_{torsion}$
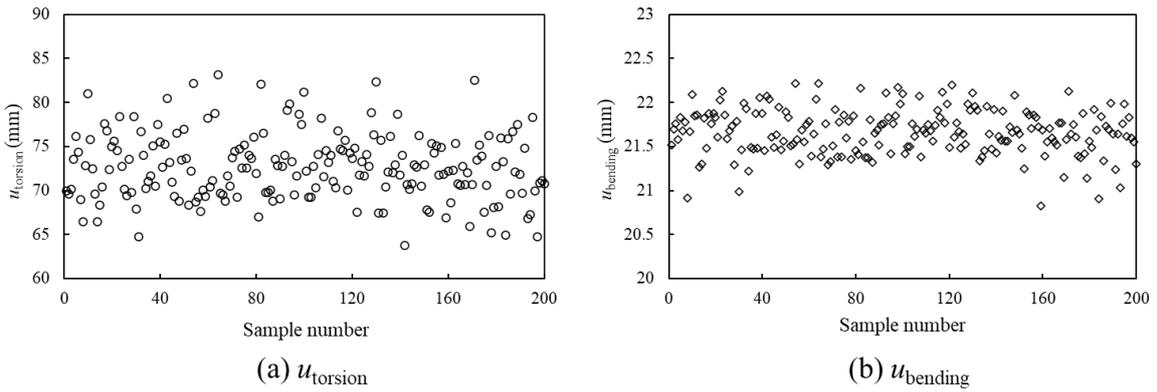
(b) $u_{bending}$

Figure 7 The distribution of $u_{torsion}$ and $u_{bending}$ from the 200 FE models for each loading scenario.
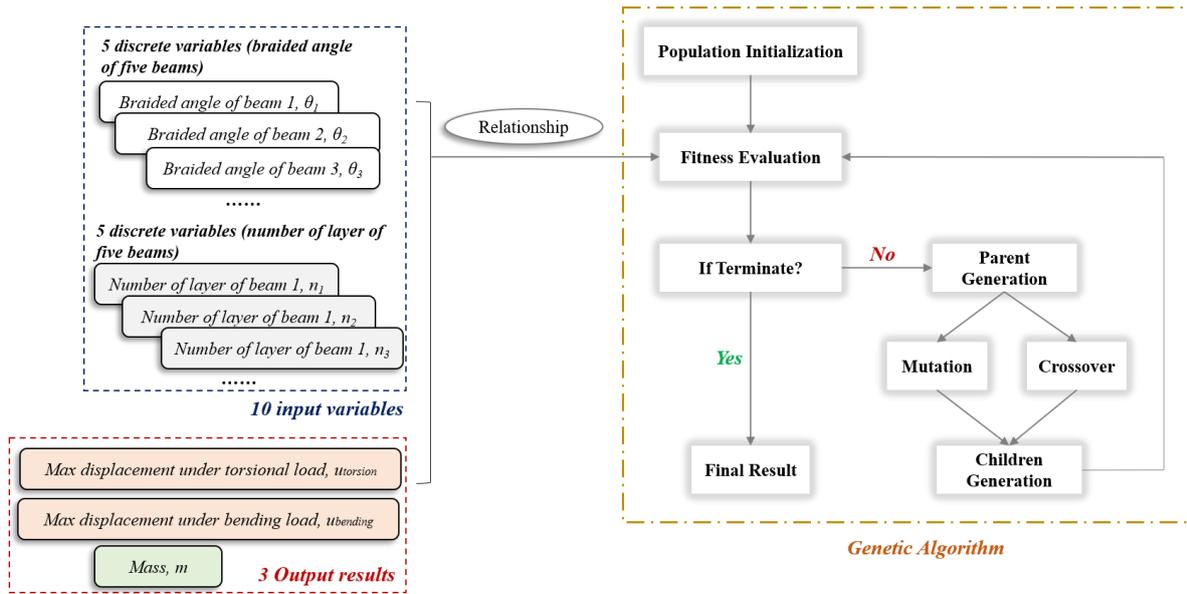
Figure 8 Flowchart of how genetic programming technique applies in this study.
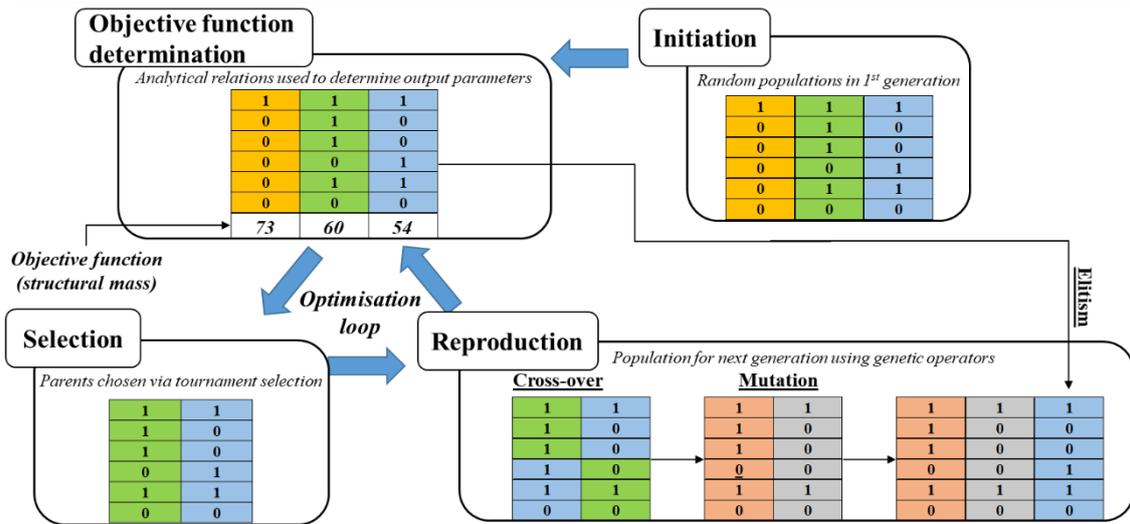
Figure 9 Flowchart representing GA-based design optimisation.
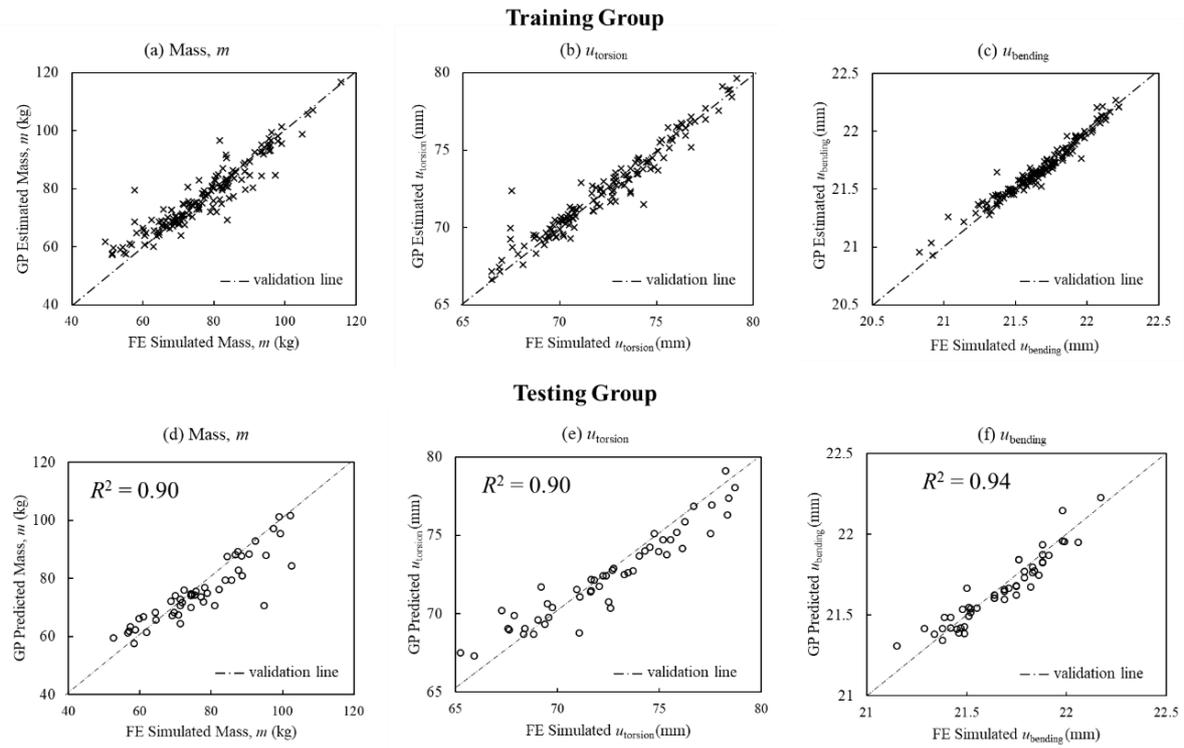
Figure 10 The correlation between GP modal predicted results and FE simulated results for training (a-c) and testing (e-f) of mass, $u_{torsion}$ and $u_{bending}$.
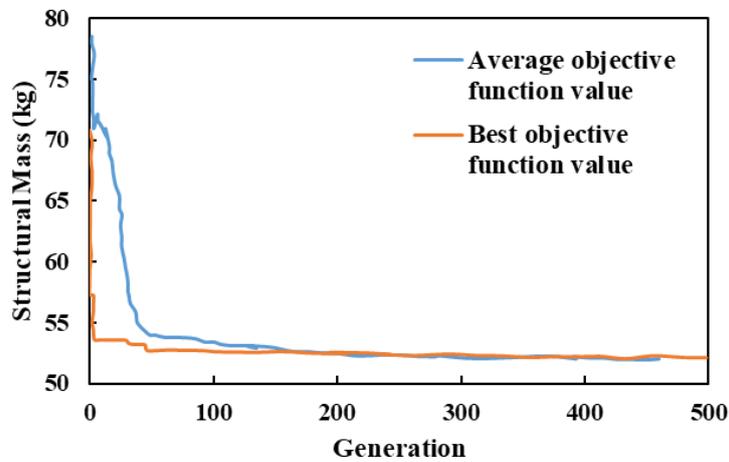
Figure 11 Objective iteration history during structural mass minimisation.

GA predicted minimum mass (52.03 kg)   Benchmark mass (61.71 kg)
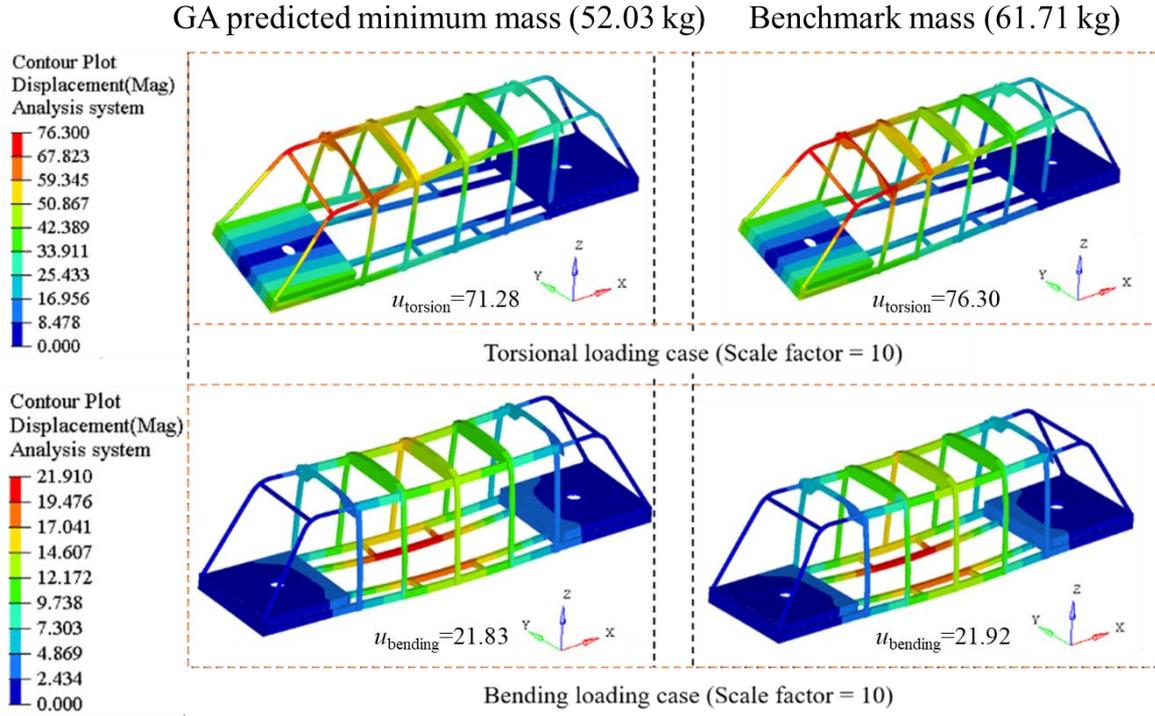
Figure 12 Obtained FE results for optimised design compared to benchmark design. Unit in mm.
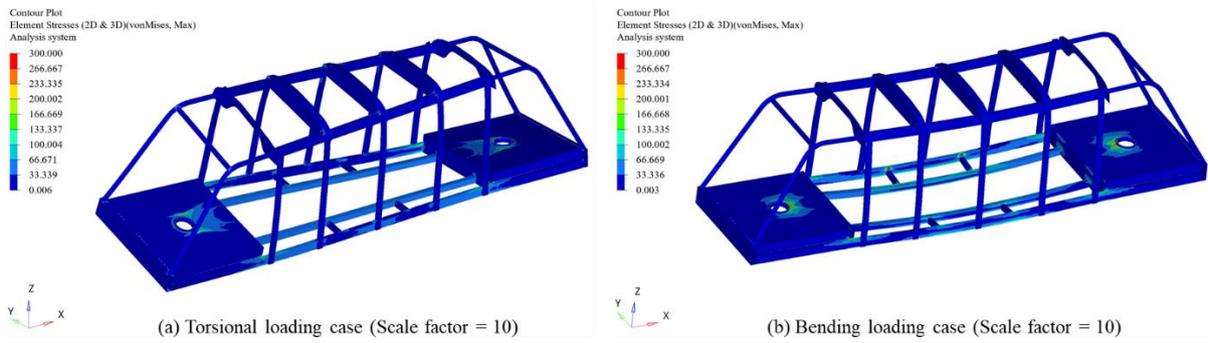
Figure 13 Stress contours of the vehicle structures for optimised design. Unit in MPa.

Table 1 Design parameters with possible values (θ is braid angle and n is number of layers). Note: i represents beam numbers from 1-5.

Design parameter	Possible values
θ_i	30º |35º | 40º | 45º | 50º | 55º |60º
n_i	3 | 4 | 5 | 6 | 7 | 8 | 9 |

Table 2 Assumed constituent properties and braiding parameters. Taken from [26].

Material properties		Braiding parameters	
E_{f1}	218.4 GPa	N	176
E_{f2}	18.1 GPa	D	108 mm
G_{f12}	21.8 GPa	Tex	800 g/km
v_{f12}	0.305		
E_m	2.89 GPa		
v_m	0.35 GPa		

Table 3 Parameters of the python programme in GPlearn.

Parameters (GPlearn)	Value
Function Set	'+', '-', '*', '/', sqrt
Population Size	8000
Generations	200
Crossover	0.7
Subtree Mutation	0.1
Hoist Mutation	0.05
Point Mutation	0.1
Parsimony Coefficient	1e-5

Table 4 GA parameters corresponding to optimisation exercise

Parameters	Value
Population Size	1500
Max generations	500
Mutation ratio	0.7

Table 5 Optimised design parameters for minimum mass of braided composite beams in the chassis

θ_1	n_1	θ_2	n_2	θ_3	n_3	θ_4	n_4	θ_5	n_5
55	8	45	3	35	4	35	3	30	8

Table 6 Comparison of the optimised design to benchmark design

	Benchmark design	Optimised design			% difference[1]
	FE simulation	GP prediction	FE simulation	% Error	
Mass (kg)	61.71	52.03	50.59	2.85	-15.69
$u_{torsion}$ (mm)	76.30	71.49	71.29	0.28	-6.30
$u_{bending}$ (mm)	21.92	21.74	21.83	0.44	-0.82
$K_{torsion}$ (N/deg)	5136.99	5482.53	5497.91	0.27	6.73
$K_{bending}$ (N/mm)	2554.74	2575.90	2565.28	0.41	0.83

[1] % difference of GP prediction of optimised design compared to FE simulation of benchmark design